NOVEL DUAL NEURAL NETWORK FOR THE CLASSIFICATION OF THE LIVER CANCER

Sunita P. Deshmukh [1]

Department of Electronics and Telecommunication, GHRU Amaravati, Amaravati, India

sunitasdeshmukh78@gmail.com

Dr. Dharmaveer Choudhari [2]

Department of Electronics and Telecommunication, GHRU Amaravati, Amaravati, India

dharmaveer.choudhari@raisoni.net

Abstract

A recently created artificial intelligence technique called deep learning (DL) can be used in many different fields. Presently, the application of DL has produced a number of impressive results for the imaging diagnosis of liver illness. The liver segmentation, lesion delineation, disease classification, process optimization, etc. are only a few of the imaging processing parts where this cutting-edge algorithm is used. Instead of a pathological biopsy, the DL optimised imaging diagnosis offers a wider perspective and has the advantages of being more convenient, safe, and affordable. In this work, researchers have suggested a unique architecture to increase classification accuracy. According to the suggested system architecture (PSA), accuracy is 98.94%. In the outcome session, the results are contrasted with those of other current algorithms.

Keywords: Deep learning, Artificial intelligence, Convolutional neural network, Liver disease, Magnetic resonance imaging, Imaging diagnosis

DOI Number: 10.14704/nq.2022.20.9.NQ440032 **Neuro Quantology 2022; 20(9):303-317**

Introduction

The liver is the major parenchymatous organ and one of the most important components of the human metabolic system [1]. This crucial organ is very susceptible and constantly experiences a variety of diffuse or localised lesions. Due to their simplicity, non-invasiveness, low cost, etc., imaging studies are genuinely crucial for the screening and diagnosis of liver illnesses even if biopsy is still the gold standard for the diagnosis of the majority of hepatic problems at present moment [2, 3]. The medical images offer objective, reliable proof for liver illnesses that may be thoroughly analysed alongside clinical symptoms and laboratory test findings. As the mainstays of imaging examinations, computed tomography (CT), magnetic resonance imaging (MRI), and ultrasound are regularly employed modalities [4–8]. However, radiologists' expert judgement, which has low sensitivity and probably exhibits observer bias, is used to evaluate the pictures [9]. Additionally, it takes a lot of labour and time to visually inspect the enormous amount of medical scans [8]. In recent years, computer-aided diagnostic (CAD) systems with computer vision (CV) and machine learning have effectively evolved for this task by enabling the interpretation of imaging rather than human segmentation and detection on the photos [10, 11]. The need for manual customisation is gradually replaced by the DL algorithm, the central element of artificial intelligence, in CAD. Contrast this with traditional machine learning approaches, which are frequently not ideal for certain tasks (Figs. 1, 2)[12, 13] and are mostly based on human developed visual descriptors.

The hierarchical representation learning architecture of DL replaces the manually constructed feature filters, processing the input data through several transformation layers with nonlinear components. The framework learns and represents the input data's features layer by layer, deriving the higher-level features from the lower-level ones [14, 15]. Convolutional neural network (CNN), auto-encoder (AE), deep belief network (DBN), and recurrent neural network (RNN) are only a few examples of the several DL designs [16–19]. These many frameworks are currently being discussed in several domains, including bioinformatics, natural language processing (NLP), and CV [20, 21]. CNN is primarily utilised for jobs involving images. CNN models are able to represent the feature maps of input data extracted by convolution kernels or compressed by pooling operation in corresponding layers by virtue of convolution layers, rectilinear units, and pooling layers sandwiched between input and output layers (Fig. 3) [23]. The feature map is produced by the convolution, which is a weighted average operation that the convolution kernel slides across the picture [24]. The activation function is then used to introduce nonlinearity, improve the model's capacity to fit data, and lessen the risk that the gradient would simultaneously vanish [25]. The feature maps are also combined in pooling layers to achieve feature down sampling and compression (Fig. 4). The fundamental framework of a CNN model is formed by the repeating and ordered arrangement of these key components. Additionally, as training progresses, gradient descent and back propagation algorithms enable the networks' parameters to self-optimize [26].

In particular, the Fully convolutional network (FCN), a variation of CNN that is favoured in several medical imaging tasks, can accept input images of any size and produce output images of the same size since all fully connected layers in the framework are replaced with convolution layers [27]. Instead of employing patch-based methods, global image analysis using FCN allows for the restoration of the original image's information. The U-Net architecture, which comprises of two symmetric components that compress and unfold the position information of pixels together with the picture attributes, is now the most often used type of FCN [28].

The training process of the DL model relies on numerous annotated data. If merely trained on limited medical data, DL models tend to suffer from both under-fitting and over-fitting problems. Generally, transfer learning is applied to medical image training of small databases. The transfer learning refers to pre-training the model on existing large databases of natural or task-related images, and the obtained network is further trained on personalized database since the features of the former layers are simi- lar in diverse image tasks empirically. Additionally, fine-tuning, which only modifies the final few layers, is always combined with transfer learning to produce results that are both speedy and precise [29, 30]. Abdominal scans frequently contain organs besides the liver, and the bulk of medical liver imaging tasks require specialised liver equipment. Due to their remarkable accuracy and short processing times, model-based segmentation algorithms have improved steadily over the past few years and are currently at the forefront of the industry.

For the purpose of segmenting the liver, FCN is the chosen model. In their study, Ben-Cohen et al. [31] suggested VGG-16 based FCN designs for the segmentation of the liver and subsequent meta-static lesion detection on CT scans. To introduce spatial information in the pre-treatment, two neighbouring slices were combined with the input axial CT scans. To bring together the various scales and bring the visual elements back to the original photos, the output layers of the models are combined with the earlier layers. With neighbouring slices, the so-called FCN-8 s architecture was able to segment the liver with a Dice index of 0.89, an average sensitivity of 0.86, and an average positive predictive value of 0.95. Another extensive coarse-to-fine method for liver segmentation was given by Zhang et al. [32], in which the liver's region of interest (ROI) is initially defined by a 2D U-net and then further refined by a 3D FCN, simultaneously providing rough tumour contours.

Additionally, frequently employed in image-guided procedures is organ segmentation. For instance, interventional scans are used to view the spatial arrangement of tools and organs during CT-guided biopsy and ablation. When lesions are not immediately obvious in the interventional image, it would be safe to merge the interventional image with the preprocedural diagnostic image. In order to segment the liver, Fang et al. [33] built a multi-scale input and multi-scale output feature abstraction network (MIMO-FAN) architecture. The segmented surfaces were then used to register the interventional CT with the preprocedural picture. Contrast-enhanced CT (CE-CT), MRI, and positron emission tomography-CT (PET-CT) registration tests revealed that the same system was effective.

For dose estimate in selective internal radiation therapy, an accurate liver segmentation is needed (SIRT). For instance, Tang et al. [34] used both CE-CT and plain CT scans for SIRT patients to develop an automatic liver segmentation approach that was modified by 3D DeepMedic. The dual-pathway framework, which has been improved, combines dense training on whole pictures with conventional patch-wise training in the CNN model. The median DSC between manual segmentation and the model for the test cohort was 0.94, and manual modification may have further improved accuracy. The liver delineation is an important preoperative step in the design of 3D imaging-assisted liver surgery. Hu et al. [35] created a 3D segmentation model and a globally optimised surface evolution algorithm for this job. The probability map of the liver is predominantly predicted by the 3D CNN in the first and second stages of the framework, and the outcome is then further refined by an energy-functional model. The energy function is adaptively integrated with the global and local information of the initial segmentation taking into consideration the changes in liver appearances. The energy function is defined in a hybrid model that includes region statistics, shape prior constraint, and gradient-edge map. The decrease of the energy function moves the anticipated surface closer to its optimal location. Regional databases and Public Segmentation of the Liver Competition 2007 (SLIVER07) were utilised to assess this tactic. On the SLIVER07 testing set, the framework achieved a mean DSC of 97.25 percent and an average symmetric surface distance of 0.84 mm, compared to the local database's 97.28 percent and 0.87 mm.

Acute liver failure, treatment planning and response evaluation, and hepatic surgery all heavily utilise analysis of the liver volume in addition to the liver's general contour [36]. Marinelli et al. [37] used a weakly supervised active transfer learning method in conjunction with additional clinical data to build the DL model for liver segmentation. In this method, the liver volume extrapolated from a clinic report by NLP replaces the standard Dice score to assess segmentation results. On the LiTS17 dataset, a 3D U-Net was trained before being applied to the Mount Sinai Health System database.

Since the model depends on a number of hyper-parameters, searching through parameter space is essential for training in DL architectures. For the purpose of segmenting the liver and classifying lesions on CT images, Ghoniem [38] merged the known DL models with the artificial bee colony (ABC) algorithm, a bio-inspired optimization technique. The model uses U-Net to extract hepatic lesions and SegNet to segment the liver. The ABC algorithm is integrated to fine-tune the hyper-parameters. On LiTS17 and another Radiopaedia database, this method was tested. The SegNet includes an encoder-decoder architectural engine that terminates at a pixel-wise classification layer, which is noteworthy. Additionally, ABC is used to optimise the hyper-parameters such as initial learning rate, maximum epochs, and minibatch size. In ABC, bee agents are a collection of computational agents, and the optimal parameters are thought of as "foods of the best quality." On the Radiopedia dataset, the suggested model attained values of 0.96, 0.968, and 0.962 for the Jac-card index, Dice index, and correlation coefficient, and values of 0.964, 0.97, and 0.958 for the same metrics on the LiTS17 database.

Table 1 contains a list of the numerous segmentation tasks for this part. The majority of the instances were tested on private databases after being tested on public ones. To assist the segmentations, several typical machine learning techniques were employed. In this upstream assignment, the vast majority of the built models performed exceptionally well overall.

Table 1. Tabular representation of research work done by different researchers

Author	Model (backbone)	Other mechanism or algorithm	Main performance	Database	Modality	References
Ben-Cohen et al.	FCN-8 s (VGG-16)	-	Dice index: 0.89, Sensitivity: 0.86, Positive predictive value: 0.95	SLIVER07, private database	Plain CT	[31]
Zhang et al.	2D slice-based U-net, 3D patch-based FCN	-	ISICDM: DSC: 96.31%, LiTS: DSC: 96.70%	ISICDM, LiTS	Plain CT	[32]
Fand et al.	MIMO-FAN	Iterative closest point algorithm, spatial pyramid pooling, deep pyramid super- vision	LiTS: Dice score: 96.1%, Speed: 0.04 s/slice	LiTS, private database	Plain CT, PET- CT, CE-CT, MRI	[33]
Tang et al.	Modified DeepMedic (CNN)	-	Test set: DSC: 0.94 (0.98 with manual correction)	SLIVER07, LiTS, Medical Segmen-tation Decathlon challenge, private database	Plain CT, CE-CT	[34]
Hu et al.	3D CNN	Globally optimized surface evolution	Sliver07: DSC: 97.2%, Average symmetric surface distance: 0.84mm	Sliver07, private database	Plain CT	[35]
Marinelli et al.	3D U-Net	Active transfer learning, NLP	MSHS: Absolute volume dif-ference: 176 ml	LiTS, private database	Plain CT	[37]
Ghoniem	SegNet-UNet-ABC	ABC algorithm	Radiopaedia: Jaccard index: 0.96, Dice index: 0.968, Correlation	LiTS, Radiopaedia	Plain CT	[38]

			coefficient: 0.962			
Yamakawa et al.	4-classification CNN(VGG-Net)	-	Accuracy: Hemangioma: 86.8%	Private database	US	[40]
Schmauch et al.	ResNet50	Attention mechanism	Weighted mean ROC-AUC score for seven different tasks of FLLs diagnosis: 0.891	Data challenge organized at the 2018 phones de Radiologie	US	[41]
Hassan et al.	stacked sparse auto encoder	Level set method, fuzzy c-means clustering algorithm	Accuracy of FLLs diagnosis: 97.2%	Private database	US	[42]
Guo et al.	DCCA-MKL	MKL	Classification of liver Accuracy: 90.41%	Private database	CEUS	[45]
Wu et al.	DBN	Sparse non-negative matrix factorizations	Classification of FLLs: Accuracy: 86.36%	Private database	CEUS	[46]
Das et al.	Watershed Gaussian based deep learning	Marker controlled watershed segmentation Gaussian mixture model algorithm	Liver cancer diagnosis: accuracy: 98.38%	Private database	Plain CT	[47]

The majority of modern CAD systems rely on classical feature engineering, which has a number of disadvantages such redundant features and high computational costs [39]. Designing manually created feature filters that are ideal for particular jobs is challenging. Matched filter is also the good choice for the removing unwanted part from medical images [54]. On the basis of US scans, Yamakawa et al. [40] built a VGG-based model for the classification of various liver cancers. The model has a 98.1 percent accuracy rate for cysts, an 86.8 percent accuracy rate for hemangiomas, an 86.3 percent accuracy rate for hepatocellular carcinoma (HCC), and a 29.2 percent accuracy rate for metastatic liver cancer. In the meantime, the team developed a binary classification model for identifying malignant lesions, whose specificity, sensitivity, and accuracy were 94.8 percent, 93.8 percent, and 94.8 percent, respectively. A DL method developed by Schmauch et al. [41] concurrently finds and identifies FLLs from liver US images.

The system incorporates an attention mechanism, and as its main component, a 50-layer ResNet that was pretrained on ImageNet was chosen. According to conventional CNN, feature extraction gives equal weight to each image point. The model's attention mechanism aids in focusing attention on the important pixels. For seven separate tasks on the testing cohort, the model finally achieved a weighted mean area under the receiver operating characteristic curve (ROC-AUC) of 0.891.

Instead of merely training on the labelled images for the many unmarked medical photos, an unsupervised algorithm is preferable to fully utilise the data. In the deep auto-encoder, the input data are compressed through the hidden layers and then restored to themselves in the output layer in order to extract latent patterns from unlabeled data. Dimensional reduction is used to save the input's latent comprehensive features. Hassan et al. [42] used a stacked sparse auto-encoder (SSAE) model to pre-train and learn the feature extraction method of the various unlabeled FLLs US images after lesion segmentation by the level set and fuzzy c-means clustering methods. To identify the various focal liver disorders, a series of auto-encoders were trained and connected to the classifier network iteratively. The SSAE system outperformed the other three comparison models, with a 97.2 percent total classification accuracy.

The contrast agent is injected into peripheral veins to enable the contrast-enhanced ultrasonography (CEUS), which was created as an improved imaging examination [43, 44]. In comparison to colour doppler US, the CEUS visualises the enhanced state of the liver, particularly for FLLs, in real-time and offers more information. This enhances FLL classification accuracy and raises the cancer detection rate. Guo et al. [45] developed a CEUS-based CAD system with multi-view learning (MKL) to categorise liver lesions in response to the extensive use of CEUS in the diagnosis of liver cancer. Atherosclerotic, portal venous, and late-phase CEUS pictures made up the system's input. This system performs a deep canonical correlation analysis (DCCA) on the pairs images after first summarising the statistical properties of the input photos. After that, an MKL classifier receives the generated findings for further analysis. In contrast to the conventional canonical correlation analysis, the DCCA employs a deep neural network (DNN) to learn the intricate nonlinear transformations of two CEUS images in an effort to identify shared information. The MKL classifier's diagnosis results had a respectable performance, and they were also very flexible and low-cost to compute. A DL diagnostic model for classifying benign and malignant FLLs using temporal intensity curves (TICs) of CEUS imaging was put forth by Wu et al. [46]. After correcting for respiratory motion, TICs of arterial and portal vein phases are extracted from dynamic CEUS videos. The final analysis revealed that the DL architecture outperformed other comparison methodologies in terms of accuracy, sensitivity, and specificity, among other quantitative criteria.

The lesions are extracted by U-Net and the LeNet-5 framework with ABC algorithm (LeNet-5/ABC) was built to extract the features of lesions and carry out the categorization in the ABC integrated technique for CT images proposed by Ghoniem et al. [38] that was previously discussed. The ABC aids in the search for the network's ideal topology. LeNet-5/ABC demonstrated pretty exceptional achievements in terms of specificity, F1-score, accuracy, and computational time, according to the results. Additionally, DL might be connected with CT's existing legacy systems. A ground-breaking Gaussian-based DL technique was created by Das et al. [47] to identify cancerous tumours in liver CT data. Marker-controlled watershed segmentation is used to segment the liver, and the Gaussian mixture model is then used to delineate the cancer lesions. Following the segmentation of the tumour, the ROI's statistical, geometrical, and texture data are combined and transmitted to a DNN for the detection of hemangiomas, HCC, and metastatic carcinoma. On the training set, this model's classification accuracy was 99.38 percent, and its Jaccard index was 98.18 percent, with approximations on the validation set.

Regarding CE-CT, each phase of which contributes significantly, the features dispersed throughout several phases serve as the image hallmark of various lesions [48]. In order to classify the FLLs utilising multi-phase CT images encompassing non-contrast, arterial, and portal venous phases, Wang et al. [49] used the fine-tuned AlexNet and 50-layer ResNet. As the input for the CNN model, the pictures from the various phases were registered to create a 3-channel image. The accuracy of AlexNet and ResNet trained with constrained medical images was found to be only 78.23% and 83.67%, respectively. Their accuracy rose to 82.94 percent and 91.22 percent when fine-tuning was included. The additional phase in a 4-phase CT scan with the delayed phase adds to radiation exposure, which may increase the risk of radiation-related pregnancies. To distinguish between HCC FLLs and non-HCC FLLs, Shi et al. [50] built a 3-phase convolutional dense network and compared it to a more traditional 4-phase network. Precontrast phase removal may improve the multi-phase CT protocol for HCC diagnosis by lowering radiation dose with DL. With accuracy rates of 85.6 percent and 83.3 percent, the results of the model without the precontrast phase were comparable to those of the 4-phase pictures, but were less accurate in distinguishing HCC from other FLLs than the model without the portal venous phase.

In addition to CT, MRI is a common imaging modality used to classify liver lesions. Using contrast-enhanced MRI, Hamm et al. [51] created and validated a CNN system for classifying hepatic lesions (CE-MRI). On another test set, the Monte Carlo cross-validation method was used to compare the DL model's accuracy to the observations of two licenced radiologists. Notably, the algorithm outperformed two radiologists' sensitivity rates of 60% and 70% by an astounding 90% when classifying HCC. With a ROC-AUC of 0.992 and a computation time of 5.6 ms per lesion, the true positive and false positive rates for all lesions in the model were 93.5 percent and 1.6 percent, respectively. The group then attempted to decipher this "black box" by associating various lesions with radiological features [52]. The 100-neuron completely connected layer of various lesions' activating patterns were observed and compared by the post hoc method, which also emphasised the input images' feature-related regions. The likelihood of a specific feature appearing in the input image was measured as a relevance score. The model with 14 representative radiological features that were carefully chosen had an accuracy of 82.9 percent in detecting the appropriate radiological features present in each test lesion and a positive predictive value of 76.5 percent. It is important to note that the integrated model is user-friendly and visualises the features of raw photos to help medical professionals explain the feature information. In a system proposed by Trivizakis et al. [53]-, to classify primary and metastatic liver carcinoma on diffusion weighted MRI (DW- MRI) as a novel input form, 3D tomographic pictures of MRI could also be used. The 3D model's accuracy was 83 percent, which was higher than the parallelly trained 2D models' accuracy of 69.6 percent and 65.2%, indicating that adding complete spatial information and building 3D models using DW-MRI are more effective approaches than using traditional models. Additionally, this 3D technique offers workable references for comparable medical imaging jobs. S. L. Bangare et al. [56-61] worked in ML and IoT domain. N. Shelke et al. [62] have proposed work for the LRA-DNN methods. S. Gupta et al. [63] has shown useful extraction methods. G. Awate et al. [64] applied the CNN methods. Xu Wu et al. [65] have proposed the network security work.

Proposed Methodology

Proposed system architecture (PCA) is the combination of two different algorithm and then the results of both algorithms get passed through the priority encoder to get the final result. In the first part there are three components to the recommended architectural technique: compression, decompression, and filtered CNN. All of the convolutions are run with appropriate padding, with the purpose of both leveraging input features and decreasing resolution by using an appropriate stride at the end of each step. The first part of the suggested architecture design is the combination of AlexNet and Unet. The second part of the PSA is extracting features by using wavelet transform and then pass those features from ANN to get the result.

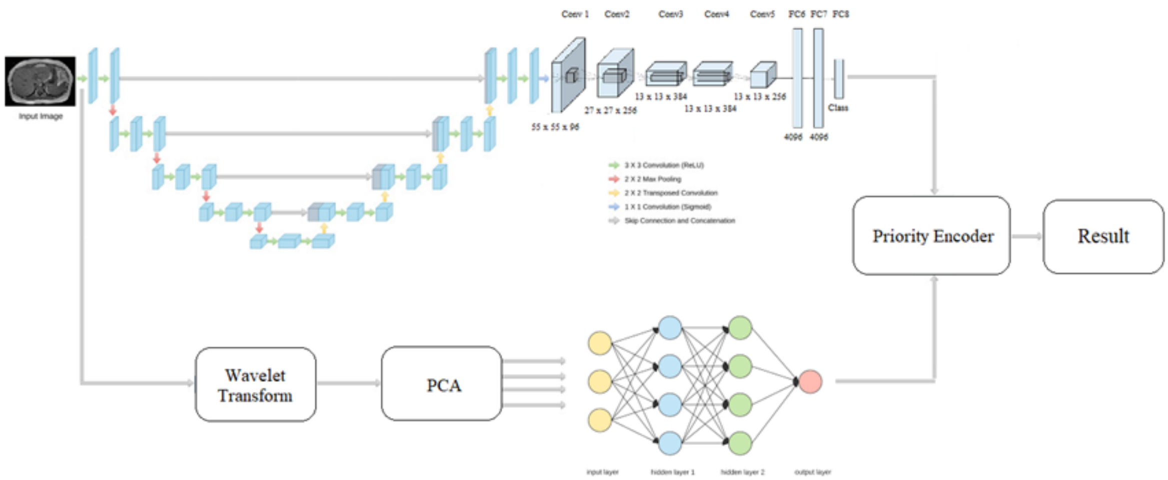

Figure 1. Proposed system architecture for the classification of the liver cancer

The image's low and high components are taken out and analysed. Three is chosen for the image's decomposition level, and Daubechies 5 is used. Equation 1 shows how the wavelet transform is applied to the $image(x, y)$ to get $W_\psi^i(j, m, n)$.

$$W_\varphi(j_0, m, n) = \frac{1}{\sqrt{MN}} \sum_{x=0}^{M-1 N-1} image(x, y)\varphi_{j=0}(x, y)$$

...equation (1)

$$W_\psi^i(j, m, n) = \frac{1}{\sqrt{MN}} \sum_{x=0}^{M=1} \sum_{y=0}^{N-1} image(x, y)\psi^i j_{j,m,n}(x, y)\psi i = \{H, V, D\}$$

...equation (2)

Here, j_0 is an arbitrary starting scale $W_\varphi(j_0, m, n)$ coefficients define an approximation of $image(x, y)$ at scale $j_0 W_\psi^i(j, m, n)$parameters for the scales $j >= j_0$ Given the W_φ and $W_\psi^i, image(x, y)$.

$$image(x, y) = \frac{1}{\sqrt{MN}} \sum_m \sum_n W_\varphi(j_0, m, n)\varphi_{j_0,m,n}(x, y) + \frac{1}{\sqrt{MN}} \sum_{i=H,V,D} \sum_{j=j_0}^{\infty} \sum_m \sum_n W_\psi^i(j, m, n)\psi_{j,m,n}^i(x, y)$$

...equation (3)

Equation 3 gives the wavelet features which then passed through the principal component analysis (PCA) to get reduced dimensionality. The statistical features are calculated and then get passed through the ANN to get the result. The statistical feature used to get the final feature set is as given in table 2.

Table 2. Description and mathematical equation of the statistical features

Property	Description	Equation
Contrast	It is the difference between the brightness of an object or region and that of its neighbouring objects or regions in the same field of view.	Contrast = $\sum_{i,j} \lvert i - j \rvert^2 p(i, j)$
Correlation	The degree and nature of the association between adjacent pixels throughout the entire image is known as correlation.	Correlation = $\sum_{i,j} \frac{(i-\mu_i)(j-\mu_j)p(i,j)}{\sigma_i \sigma_j}$
Energy	A few different shades of grey make up an energy, which measures how homogenous an image is.	Energy = $\sum_{i,j} p(i, j)^2$
Homogeneity	The degree of homogeneity describes how closely a matrix's element distribution resembles its diagonal matrix.	Homogeneity = $\sum_{i,j} \frac{p(i,j)}{1+\lvert i-j \rvert}$

Mean	It represents an average of the pixel-level brightness in the area. It calculates a region's pixel density as an indicator of the brightness of that area on average.	$\mu = \sum_{i=0}^{G-1} i\,p(i)$
Variance	This gauges how widely an image's intensity deviates from its mean.	$\sigma^2 = \sum_{i=0}^{G-1} (i-\mu)^2\,p(i)$
Skewness	Skewness is a measure of asymmetry that is 0 when a histogram is symmetric about the mean; otherwise, it can be either positive or negative depending on whether the histogram is skewed above or below the average.	$\mu_3 = \sigma^{-3} = \sum_{i=0}^{G-1} (i-\mu)^3\,p(i)$
Kurtosis	It gauges how flat a histogram or peak distribution is in comparison to a normal distribution.	$\mu_4 = \sigma^{-4} = \sum_{i=0}^{G-1} ((i-\mu)^4\,p(i)) - 3$
Entropy	It serves as a gauge for the overall disorder or randomness of the image.	$E = -\sum_{i=0}^{G-1} p(i)\log_2[p(i)]$

These features are then passed through the statistical analysis process. The obtained result from first and second part of the PSA is passed through the priority encoder. The highest priority if set to the class “Cholangiocarcinoma” and on the second priority there is class with name “Normal” and the third class is of “Hepatoblastoma”. The result obtained from the first part of the PSA and the result obtained from the second part of the PSA is then according to the priority of the class is selected as a output.

Result and Discussion

There are various types of malignant growths in the liver. The malignant growths known as cholangiocarcinoma and hepatoblastoma frequently fascinate the scientists in this review. Using 2871 images, the framework's exhibition is evaluated. A Dual Hybrid Model was used by the scientists to achieve excellent precision. A final decision on picture order is made by the Result Prioritizer using the output of both neural networks. The ultimate result is that indistinguishable consequence, assuming that both neural organisations' results are equivalent (which is typically the case). In the Alexnet and Unet method, the image is first subjected to a wavelet transformation, and the resulting image is then handled by a crossbreed (Alexnet and Unet) neural organisation model. As a result, an order is obtained. The CNN method does the equivalent to the wavelet change, after which the picture's components are recovered. To condense the length of those features, PCA is used. The information is then handled into the CNN to obtain a result under the assumption that the outcomes of the two neural organisations differ; the outcome is still up in the air depending on necessity. For instance, Hepatoblastoma is given the least attention, whereas Cholangiocarcinoma receives the best requirement. Overall, regardless of which neural organisation produced the outcome, if any of the neural organisations produce a Cholangiocarcinoma result, Cholangiocarcinoma is the final consequence. Figure 2 shows the confusion matrix of the result of classification using PSA followed by table 3 showing performance parameters of the same.

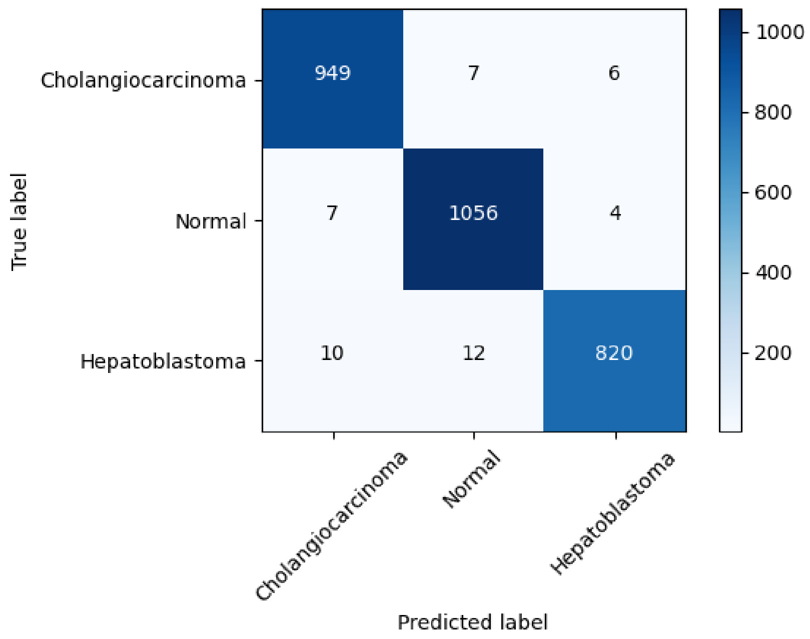

Figure 2. Confusion matrix of PSA

Table 3. the performance parameters of the classification using PSA

	Cholangiocarcinoma	Normal	Hepatoblastoma	Overall
Accuracy	98.96%	98.96%	98.89%	0.989366667
Precision	99%	99%	97%	0.983333333
Recall	98%	98%	99%	0.983333333
F1 score	98%	99%	98%	0.983333333

The graphical representation of the performance parameters are shown in figure 3 which only shows that every performance parameter higher that 97%.

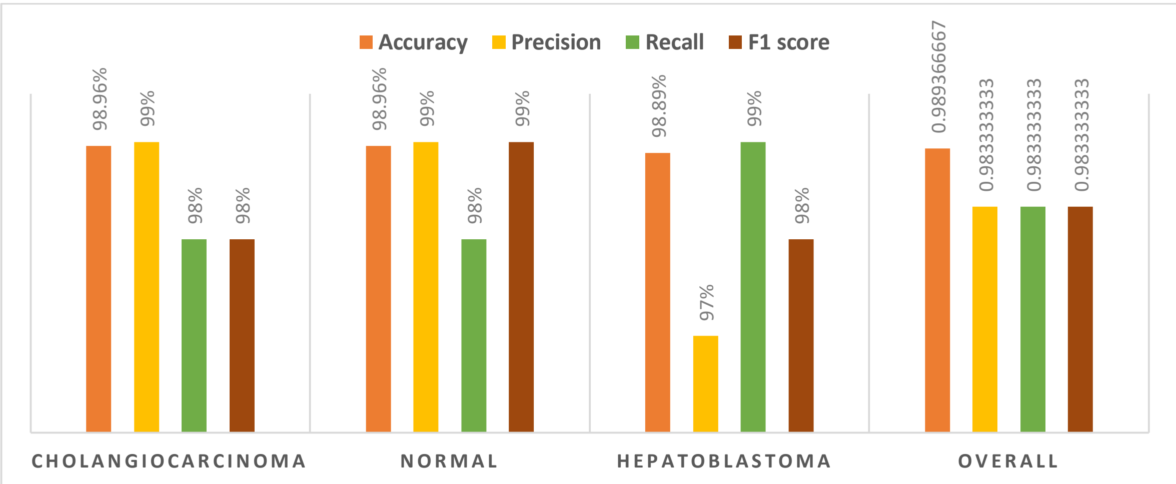

Figure 3. Graphical representation of the performance parameters of the PSA

The PSA is compared with the other existing systems with respect to performance parameters which are as tabulated in table 4.

Table 4. Comparison of the PSA with other existing algorithms on the basis of performance parameters

	Accuracy	Precision	Recall	F1 score
PSA	98.94	98.33	98.33	98.33
AlexNet	97.342	95.24	95.41	95.23
U-Net	95.744	92.15	92.49	92.13
V-Net	94.146	89.06	89.57	89.03
CNN	89.31	87.32	84.12	83.12
Yolo V3	90.95	82.88	83.73	82.83
SVM	89.352	79.79	80.81	73.12
Random Forest	75.31	74.12	73.12	76.63
Decision Tree	86.156	73.61	74.97	71.32

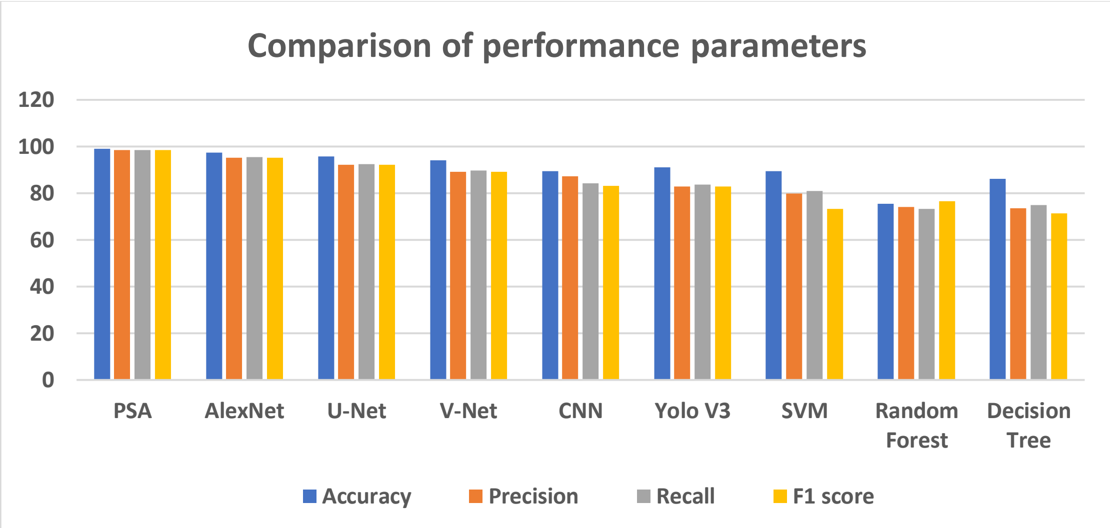

Figure 4. comparison of performance parameters of different algorithms

The results presented in table 4 along with figure 4 gives the better idea about how PSA is better than other algorithms. Every performance parameter of the PSA is superior amongst all other algorithms.

Additionally, the time complexity of the various processors is examined. The average turnaround time for various hardware systems is compiled in table 5.

Table 5. The time it takes to get the result by using PSA on different hardware platforms [55]

Platform	Time required to get result (in seconds)
CPU, i3 processor, 8GB RAM	0.293
CPU, i5 processor, 8GB RAM	0.193
CPU, I7 processor, 8GB RAM	0.191
GPU, Nvidia K80	0.0026

The use of CPU, i5 and the i7 gives almost same time complexity, but when the system is tested on GPU then there is huge difference in time required to get the results.

Conclusion

This paper proposes a revolutionary method for recognising and dissecting sores and liver disease. A few layers of the brain organisation are used to extract the characteristics of clinical pictures in order to improve the accuracy of clinical picture distinguishing proof. DWT is a tool for pre-handling images. Using the PCA method, some quantitative boundaries from pre-handled images are removed, including mean, middle, standard deviation, skewness, and kurtosis. CNN is used to consider and assess the measurably available factors. There are various types of malignant growths in the liver. The scientists doing this review find the malignant cholangiocarcinoma and hepatoblastoma growths to be particularly intriguing. Utilizing 2871 images, the framework's exhibition is reviewed. The experts achieved amazing precision using a Dual Hybrid Model. The Result Prioritizer, which ultimately decides on picture order, is currently provided the results of both neural organisations. If both neuronal organisations' effects are comparable, which they are in most cases, then the same result becomes the final result at that time. In the Alexnet and Unet method, the image is first subjected to a wavelet transformation, and the resulting image is then handled by a hybrid (Alexnet and Unet) neural organisation model. The CNN approach for recovering picture quality also makes use of the wavelet change. To condense the range of such features, PCA is used. The information is then sent into CNN, which produces a result. If the outcomes of the two neuronal organisations differ, the decision will not necessarily be made based on precedence. When the PSA's performance metrics are compared to those of other algorithms, it becomes clear that the PSA is the best algorithm.

References

[1] Trefts E, Gannon M, Wasserman DH. The liver. Curr Biol 2017;27(21):R1147–R1151

[2] Di Tommaso L, et al. Role of liver biopsy in hepatocellular carcinoma. World J Gastroenterol 2019;25(40):6041–6052

[3] Ayuso C, et al. Diagnosis and staging of hepatocellular carcinoma (HCC): current guidelines. Eur J Radiol 2018; 101:72–81

[4] Sertorio F, et al. Ultrasonography as first line imaging for the diag- nosis of positional plagiocephaly: our experience and literature review. Minerva Pediatr 2019. https://doi.org/10.23736/S0026-4946.19.05424-0

[5] Nishida N, et al. Current status and perspectives for computer- aided ultrasonic diagnosis of liver lesions using deep learning technology. Hepatol Int 2019;13(4):416–421

[6] Choi KJ, et al. Development and validation of a deep learning system for staging liver fibrosis by using contrast agent-enhanced CT images in the liver. Radiology 2018;289(3):688–697

[7] Han X. MR-based synthetic CT generation using a deep convolu- tional neural network method. Med Phys 2017;44(4):1408–1419

[8] Ben-Cohen A, Greenspan H. Liver lesion detection in CT using deep learning techniques. In: Handbook of Medical Image Com- puting and Computer Assisted Intervention, 2020; p. 65–90. https://doi.org/10.1016/B978-0-12-816176-0.00008-9

[9] Waite S, et al. Interpretive error in radiology. AJR Am J Roent- genol 2017;208(4):739–749

[10] Chan HP, Samala RK, Hadjiiski LM. CAD and AI for breast cancer-recent development and challenges. Br J Radiol 2020;93(1108):20190580

[11] Suzuki K. Overview of deep learning in medical imaging. Radiol Phys Technol 2017;10(3):257–273

[12] Sapkota M, Shi X, Xing F, Yang L. Deep convolutional hash- ing for low-dimensional binary embedding of histopathological images. IEEE J Biomed Health Inf 2019;23(2):805–816

[13] Le EPV, et al. Artificial intelligence in breast imaging. Clin Radiol 2019;74(5):357–366

[14] Sahiner B, et al. Deep learning in medical imaging and radiation therapy. Med Phys 2019;46(1):e1–36

[15] Lundervold AS, Lundervold A. An overview of deep learn- ing in medical imaging

focusing on MRI. Z Med Phys 2019;29(2):102–127
[16] Sarıgül M, Ozyildirim BM, Avci M. Differential convolutional neural network. Neural Netw 2019; 116:279–287
[17] Karim AM, et al. A novel framework using deep auto-encod- ers based linear model for data classification. Sensors (Basel) 2020;20(21):6378
[18] Movahedi F, Coyle JL, Sejdic E. deep belief networks for electroencephalography: a review of recent contributions and future outlooks. IEEE J Biomed Health Inf. 2018;22(3):642–652
[19] Barak O. Recurrent neural networks as versatile tools of neurosci- ence research. Curr Opin Neurobiol 2017;46:1–6
[20] Pons E, Braun LM, Hunink MG, Kors JA. Natural language processing in radiology: a systematic review. Radiology 2016;279(2):329–343
[21] Min S, Lee B, Yoon S. Deep learning in bioinformatics. Brief Bioinform 2017;18(5):851–869
[22] Huan EY, Wen GH. Multilevel and multiscale feature aggregation in deep networks for facial constitution classification. Comput Math Methods Med 2019; 2019:1258782
[23] Yamashita R, Nishio M, Do RKG, Togashi K. Convolutional neu- ral networks: an overview and application in radiology. Insights Imaging 2018;9(4):611–629
[24] Biswas M, et al. Symtosis: A liver ultrasound tissue characteriza- tion and risk stratification in optimized deep learning paradigm. Comput Methods Programs Biomed 2018;155:165–177
[25] Ohn I, Kim Y. Smooth function approximation by deep neural networks with general activation functions. Entropy (Basel) 2019;21(7):627
[26] Soffer S, et al. Convolutional neural networks for radiologic images: a radiologist's guide. Radiology 2019;290(3):590–606
[27] Shelhamer E, Long J, Darrell T. Fully convolutional networks for semantic segmentation. IEEE Trans Pattern Anal Mach Intell 2017;39(4):640–651
[28] Falk T, et al. U-Net: deep learning for cell counting, detection, and morphometry. Nat Methods 2019;16(1):67–70
[29] Clancy K, et al. Deep learning pre-training strategy for mammo- gram image classification: an evaluation study. J Digit Imaging 2020;33(5):1257–1265
[30] Jansen MJA, et al. Patient-specific fine-tuning of convolutional neural networks for follow-up lesion quantification. J Med Imag- ing (Bellingham) 2020;7(6):064003
[31] Ben-Cohen A, et al. Fully convolutional network for liver segmen- tation and lesions detection. Deep Learn Data Label Med Appl 2016. https://doi.org/10.1007/978-3-319-46976-8_9

[32] Zhang Y, et al. Deep learning initialized and gradient enhanced Level-Set based segmentation for liver tumor from CT images. IEEE Access 2020;8:76056–76068
[33] Fang X, Xu S, Wood BJ, Yan P. Deep learning-based liver seg- mentation for fusion-guided intervention. Int J Comput Assist Radiol Surg 2020;15(6):963–972
[34] Tang X, et al. Whole liver segmentation based on deep learning and manual adjustment for clinical use in SIRT. Eur J Nucl Med Mol Imaging 2020;47(12):2742–2752
[35] Hu P, et al. Automatic 3D liver segmentation based on deep learn- ing and globally optimized surface evolution. Phys Med Biol 2016;61(24):8676–8698
[36] Winkel DJ, et al. Validation of a fully automated liver segmen- tation algorithm using multi-scale deep reinforcement learn- ing and comparison versus manual segmentation. Eur J Radiol 2020;126:108918
[37] Marinelli B, et al. Combination of active transfer learning and natural language processing to improve liver volumetry using sur- rogate metrics with deep learning. Radiol Artif Intell 2019. https://doi.org/10.1148/ryai.2019180019
[38] Ghoniem RM. A novel bio-inspired deep learning approach for liver cancer diagnosis. Information 2020;11(2):80
[39] Halder A, Dey D, Sadhu AK. lung nodule detection from feature engineering to deep learning in thoracic CT images: a compre- hensive review. J Digit Imaging 2020;33(3):655–677
[40] Yamakawa M, Shiina T, Nishida N, Kudo M. Computer aided diagnosis system developed for ultrasound diagnosis of liver lesions using deep learning. In: 2019 IEEE International Ultra- sonics Symposium (IUS), 2019; p. 2330–2333. https://doi.org/10.1109/ULTSYM.2019.8925698

[41] Schmauch B, et al. Diagnosis of focal liver lesions from ultrasound using deep learning. Diagn Interv Imaging 2019;100(4):227–233
[42] Hassan TM, Elmogy M, Sallam ES. Diagnosis of focal liver dis- eases based on deep learning technique for ultrasound images. Arab J Sci Eng 2017;42:3127–3140
[43] Durot I, Wilson SR, Willmann JK. Contrast-enhanced ultra- sound of malignant liver lesions. Abdom Radiol (NY) 2018;43(4):819–847
[44] Jaspers N, Pfister R, Kinkel H, Michels G. Kontrastmittelsonog- raphie [Contrast-enhanced ultrasound]. Dtsch Med Wochenschr 2012;137(45):2336–2339
[45] Guo L, et al. CEUS-based classification of liver tumors with deep canonical correlation analysis and multi-kernel learning. In: 2017 39th Annual International Conference of the IEEE Engineering in Medicine and Biology Society (EMBC), 2017; p. 1748–1751. https://doi.org/10.1109/EMBC.2017.8037181
[46] Wu K, Chen X, Ding MY. Deep learning based classification of focal liver lesions with contrast-enhanced ultrasound. Optik 2014;125(15):4057–4063
[47] Das A, et al. Deep learning based liver cancer detection using watershed transform and Gaussian mixture model techniques. Cogn Syst Res 2019;54:165–175
[48] Xu X, et al. Radiomic analysis of contrast-enhanced CT predicts microvascular invasion and outcome in hepatocellular carcinoma. J Hepatol 2019;70(6):1133–1144
[49] Wang W, et al. Classification of focal liver lesions using deep learning with fine-tuning. In: Proceedings of the 2018 Interna- tional Conference on digital medicine and image processing 2018; p. 56–60. https://doi.org/10.1145/3299852.3299860
[50] Shi W., et al. Deep learning assisted differentiation of hepatocel- lular carcinoma from focal liver lesions: choice of four-phase and three-phase CT imaging protocol. Abdom Radiol (NY) 2020;45(9):2688–2697
[51] Hamm CA, et al. Deep learning for liver tumor diagnosis part I: development of a convolutional neural network classifier for multi-phasic MRI. Eur Radiol 2019;29(7):3338–3347
[52] Wang C, et al. Deep learning for liver tumor diagnosis part II: con- volutional neural network interpretation using radiologic imaging features. Eur Radiol 2019;29(7):3348–3357
[53] Trivizakis E, et al. Extending 2-D convolutional neural networks to 3-D for advancing deep learning cancer classification with application to mri liver tumor differentiation. IEEE J Biomed Health Inf 2019;23(3):923–930
[54] A. S. Ladkat, S. S. Patankar and J. V. Kulkarni, "Modified matched filter kernel for classification of hard exudate," 2016 International Conference on Inventive Computation Technologies (ICICT), 2016, pp. 1-6, doi: 10.1109/INVENTIVE.2016.7830123.
[55] A. S. Ladkat, A. A. Date and S. S. Inamdar, "Development and comparison of serial and parallel image processing algorithms," 2016 International Conference on Inventive Computation Technologies (ICICT), 2016, pp. 1-4, doi: 10.1109/INVENTIVE.2016.7824894.
[56] S. L. Bangare, "Classification of optimal brain tissue using dynamic region growing and fuzzy min-max neural network in brain magnetic resonance images", Neuroscience Informatics, Volume 2, Issue 3, September 2022, 100019, ISSN 2772-5286, https://doi.org/10.1016/j.neuri.2021.100019.
[57] S. L. Bangare, G. Pradeepini, S. T. Patil, "Implementation for brain tumor detection and three dimensional visualization model development for reconstruction", ARPN Journal of Engineering and Applied Sciences (ARPN JEAS), Vol.13, Issue.2, ISSN 1819-6608, pp.467-473. 20/1/2018 http://www.arpnjournals.org/jeas/research_papers/rp_2018/jeas_0118_6691.pdf
[58] Sunil L. Bangare, Deepali Virmani, Girija Rani Karetla, Pankaj Chaudhary, Harveen Kaur, Syed Nisar Hussain Bukhari, and Shahajan Miah, "Forecasting the Applied Deep Learning Tools in Enhancing Food Quality for Heart Related Diseases Effectively: A Study Using Structural Equation Model Analysis", Hindawi Journal of Food Quality, Volume 2022, Article ID 6987569, 8 pages, https://doi.org/10.1155/2022/6987569
[59] S. L. Bangare, G. Pradeepini, S. T. Patil et al, "Neuroendoscopy Adapter Module

Development for Better Brain Tumor Image Visualization", International Journal of Electrical and Computer Engineering (IJECE) Vol. 7, No. 6, December 2017, pp. 3643~3654. http://ijece.iaescore.com/index.php/IJECE/article/view/8733/7392

[60] S. L. Bangare, G. Pradeepini and S. T. Patil, "Brain tumor classification using mixed method approach," 2017 International Conference on Information Communication and Embedded Systems (ICICES), 2017, pp. 1-4, doi: 10.1109/ICICES.2017.8070748.

[61] S. L. Bangare, S. Prakash, K. Gulati, B. Veeru, G. Dhiman and S. Jaiswal, "The Architecture, Classification, and Unsolved Research Issues of Big Data extraction as well as decomposing the Internet of Vehicles (IoV)," 2021 6th International Conference on Signal Processing, Computing and Control (ISPCC), 2021, pp. 566-571, doi: 10.1109/ISPCC53510.2021.9609451.

[62] N. Shelke, S. Chaudhury, S. Chakrabarti, S. L. Bangare et al. "An efficient way of text-based emotion analysis from social media using LRA-DNN", Neuroscience Informatics, Volume 2, Issue 3, September 2022, 100048, ISSN 2772-5286, https://doi.org/10.1016/j.neuri.2022.100048.

[63] Suneet Gupta, Sumit Kumar, Sunil L. Bangare, Shibili Nuhmani, Arnold C. Alguno, Issah Abubakari Samori, "Homogeneous Decision Community Extraction Based on End-User Mental Behavior on Social Media", Computational Intelligence and Neuroscience, vol. 2022, Article ID 3490860, 9 pages, 2022. https://doi.org/10.1155/2022/3490860.

[64] Gururaj Awate, S. L. Bangare, G. Pradeepini and S. T. Patil, "Detection of Alzheimers Disease from MRI using Convolutional Neural Network with Tensorflow", arXiv, https://doi.org/10.48550/arXiv.1806.10170

[65] Xu Wu, Dezhi Wei, Bharati P. Vasgi, Ahmed Kareem Oleiwi, Sunil L. Bangare, and Evans Asenso, "Research on Network Security Situational Awareness Based on Crawler Algorithm", Security and Communication Networks, Hindawi, ISSN:1939-0114, E-ISSN:1939-0122, https://www.scopus.com/sourceid/18000156707.